J. Fluid Mech. (2007), *vol.* 589, *pp.* 57–81. © 2007 Cambridge University Press
doi:10.1017/S0022112007007495 Printed in the United Kingdom

Velocity and temperature derivatives in high-Reynolds-number turbulent flows in the atmospheric surface layer. Part 1. Facilities, methods and some general results

G. GULITSKI[1], M. KHOLMYANSKY[1], W. KINZELBACH[2], B. LÜTHI[2], A. TSINOBER[1] AND S. YORISH[1]

[1]Faculty of Engineering, Tel Aviv University, Tel Aviv 69978, Israel

[2]Institute of Environmental Engineering, ETH Zürich, CH-8093 Zürich, Switzerland

(Received 11 January 2006 and in revised form 19 May 2007)

This is a report on a field experiment in an atmospheric surface layer at heights between 0.8 and 10 m with the Taylor micro-scale Reynolds number in the range $Re_\lambda = 1.6 - 6.6 \times 10^3$. Explicit information is obtained on the full set of velocity and temperature derivatives both spatial and temporal, i.e. no use of Taylor hypothesis is made. The report consists of three parts. Part 1 is devoted to the description of facilities, methods and some general results. Certain results are similar to those reported before and give us confidence in both old and new data, since this is the first repetition of this kind of experiment at better data quality. Other results were not obtained before, the typical example being the so-called tear-drop $R-Q$ plot and several others. Part 2 concerns accelerations and related matters. Part 3 is devoted to issues concerning temperature, with the emphasis on joint statistics of temperature and velocity derivatives. The results obtained in this work are similar to those obtained in experiments in laboratory turbulent grid flow and in direct numerical simulations of Navier–Stokes equations at much smaller Reynolds numbers $Re_\lambda \sim 10^2$, and this similarity is not only qualitative, but to a large extent quantitative. This is true of such basic processes as enstrophy and strain production, geometrical statistics, the role of concentrated vorticity and strain, reduction of nonlinearity and non-local effects. The present experiments went far beyond the previous ones in two main respects. (i) All the data were obtained without invoking the Taylor hypothesis, and therefore a variety of results on fluid particle accelerations became possible. (ii) Simultaneous measurements of temperature and its gradients with the emphasis on joint statistics of temperature and velocity derivatives. These are reported in Parts 2 and 3.

1. Introduction

The work reported in the present paper is based on two premises: (i) we need information on velocity and temperature derivatives; and (ii) we need this and other information at large Reynolds numbers.

Velocity derivatives, $A_{ij} = \partial u_i/\partial x_j$, are known to play a major role in the dynamics of turbulence for a number of reasons. Their importance has become especially clear since the papers by Taylor (1937, 1938) and Kolmogorov (1941*a*, *b*). Taylor emphasized the role of vorticity, i.e. the antisymmetric part of the velocity gradient tensor, $A_{ij} = \partial u_i/\partial x_j$, whereas Kolmogorov stressed the importance of dissipation, and

thereby of strain, i.e. the symmetric part of the tensor A_{ij}. Fluid particle acceleration is another important kind of velocity derivatives (see Vedula & Yeung 1999; Tsinober, Vedula & Yeung 2001; Vedula, Yeung & Fox 2001; Mordant *et al.* 2003, 2004*a–c*; Crawford, Mordant & Bodenschatz 2005, and references therein).

Among the main difficulties in turbulence research in general, and applications in particular, is that the high values of Reynolds numbers are inaccessible for the foreseeable future either in the laboratory or via direct numerical simulations. On the other hand, information on such turbulent flows is important both for basic research and applications. This information includes all three components of turbulent velocity fluctuations, u_i, all nine components of the spatial velocity gradients tensor, $\partial u_i/\partial x_j$, and its time derivatives, $\partial u_i/\partial t$, with synchronous data on fluctuations of temperature, θ, its spatial gradient, $\partial\theta/\partial x_j$, and temporal derivative, $\partial\theta/\partial t$, along with the corresponding data on the mean flow. Having such information allows us to address a number of important issues associated with vorticity and strain, vortex stretching and enstrophy production, surrogates versus true quantities, geometrical statistics, properties of fluid particle accelerations and random Taylor hypothesis, and a number of key issues of the behaviour of passive scalars in large-Reynolds-number turbulent flows, which up to recently were essentially inaccessible, such as joint statistical properties of the field of velocity derivatives, i.e. rate of strain tensor, s_{ij}, and vorticity, ω_i, and the temperature gradient, $\partial\theta/\partial x_j$.

The central goal of this work is to question how large the Reynolds numbers must be in order to study the basic physics of turbulence. It appears that the high-Reynolds-number results are qualitatively, if not quantitatively, the same as previous low-Reynolds-number results, i.e. it is not always necessary to have high Reynolds numbers in order to study the basic physics of turbulence. This means that the importance of concepts such as inertial range were probably overstressed. Thus, it will not always be necessary to push to higher Reynolds numbers for experiments and direct numerical simulation (DNS). Our main technical aims were to improve various components of the experimental facility. The most important of these is the possibility of employing the multi-hot-wire technique without invoking the Taylor hypothesis, and thereby accessing the fluid particle accelerations and a variety of its Eulerian components, with simultaneous access to temperature and its derivatives. This makes it possibile to obtain joint statistics of velocity and temperature gradients experimentally.

In order to achieve reasonably high Reynolds numbers and access velocity derivatives, it is necessary to perform field experiments, as reported by Kholmyansky & Tsinober (2000), Kholmyansky *et al.* (2000, 2001*a*, *b*) and Galanti *et al.* (2003). Though most of these experiments were performed using the Taylor hypothesis, a successful attempt was made to check the possibility of measuring all spatial derivatives without invoking the Taylor hypothesis (Kholmyansky *et al.* 2001*b*). A similar experiment with simultaneous measurements of temperature fluctuations and their spatial derivatives was performed by Galanti *et al.* (2003). This opened the possibility of accessing the corresponding temporal derivatives and consequently the fluid particle accelerations.

The field experiments mentioned above were performed on the ground of the Kfar Glikson kibbutz, a few kilometres to the north-east of Pardes-Hanna, Israel. The wind at this site, that was good with regard to wind velocity and topography, had a large directional variability (see below), leading to reduced data quality. The bulk of the results reported below were obtained at the Sils-Maria site in Switzerland which had a more stable wind direction.

Our report is divided into three parts. Part 1 is devoted to the description of facilities, methods and some general results of two kinds. The first kind are results

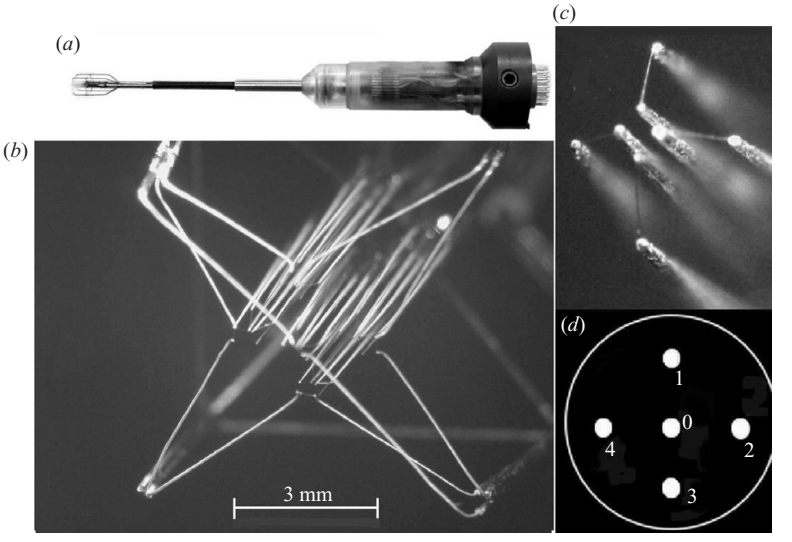

FIGURE 1. The multi-hot/cold-wire probe. (*a*) Assembled probe. (*b*) Micro-photograph of the tip of the probe. (*c*) Tip of individual hot-wire array. (*d*) Schematic of the position of the arrays 1–4 relative to the central array 0.

similar to those reported before (Kholmyansky & Tsinober 2000; Kholmyansky *et al.* 2000, 2001*a*, *b*; Galanti *et al.* 2003). They give us confidence in both experiments, since it is the first repetition of this kind of experiment at better data quality. The second kind are the results which were not obtained previously, the typical example being the so-called tear-drop $R - Q$ plot and several others.

Part 2 (Gulitski *et al.* 2007*a*) concerns accelerations and related matters. It includes a variety of results on convective, local and other 'components' of fluid particle accelerations, such as variances, correlations and geometrical statistics. Part 3 (Gulitski *et al.* 2007*b*), is devoted to issues concerning temperature, with the emphasis on joint statistics of temperature and velocity derivatives.

2. Experiments

The results described below are based on the data obtained in field experiments in the atmospheric surface layer, and in laboratory experiments with a jet facility. The measurement system used allows us to obtain all three components of the velocity fluctuations vector, u_i, all nine components of the spatial velocity gradient tensor, $\partial u_i/\partial x_j$, and the temporal velocity derivatives, $\partial u_i/\partial t$, with synchronous data on fluctuations of temperature, θ, its spatial gradient, $\partial\theta/\partial x_j$, and temporal derivative, $\partial\theta/\partial t$, along with corresponding data on the mean flow.

The most essential components of the experimental system are a multi-hot/cold-wire probe, a 20-channel hot-wire anemometer, a 5-channel cold-wire thermometer, a data acquisition and processing system and an automatic three-dimensional calibration unit with corresponding calibration procedure, including software.

2.1. *Probe*

The basic element of our multi-wire probe (figure 1) is an array. It consists of four hot-wires, forming a pyramid. Each wire is welded to a pair of prongs, providing support and electrical connection for the hot wires (figure 1*c*). The typical length of

a wire is 0.6 mm, its diameter is 2.5 μm. The diameter of a typical array is a little less than 1 mm, and the separation between the arrays is 1.2 mm. Each wire is connected to a separate channel of a hot-wire anemometer. Five parallel arrays, combined in a cross-like configuration (figure 1*d*), form a probe.

Each array of the calibrated probe gives three components of the velocity vector, that can be related to a certain point in the tip of the array. The distance between the arrays is small (overall size of the tip of the probe is about 3 mm, i.e. less then five Kolmogorov scales under the flow conditions described in Kholmyansky *et al.* (2001*a*, *b*). In the reported measurements the Kolmogorov length was in the range 0.35—0.76 mm, see table 1. Hence the tip of the probe was from 3.9 to 8.6 Kolmogorov lengths.) Therefore the differences between the values of the velocity components from properly chosen arrays can be used to estimate lateral and vertical space derivatives. The space derivatives in the longitudinal direction can be obtained from time differences, using the Taylor hypothesis.

Such a probe was successfully implemented in laboratory and field experiments (Tsinober *et al.* 1992, 1997; Kholmyansky & Tsinober 2000; Kholmyansky *et al.* 2001*a*, *b*). Though the probe, which consists of 20 hot wires in five four-wire arrays, seems to be 'crowded' with many wires and prongs, it does not cause more serious flow disturbances than the usual hot-wire probes (see, e.g. Tsinober *et al.* 1992). Indeed, it is essentially empty: the volume of solid material in the proximity of the probe tip is only about 1 % of the volume of the tip. This is achieved mainly by using thin prongs with tips of about 0.025 mm thickness (figure 1).

Several essentially new developments and significant improvements were introduced in the probe as compared to the previous experiments (Kholmyansky & Tsinober 2000; Busen *et al.* 2001; Kholmyansky *et al.* 2001*a*, *b*). The first one is a probe allowing to estimate the spatial derivative in the streamwise direction independently of the time derivative, i.e. without invoking the Taylor hypothesis (Kholmyansky *et al.* 2001*b*; Galanti *et al.* 2003). This is achieved by designing a five-array probe with the central array shifted forward in the streamwise direction by approximately 1 mm. Such a probe allows us to estimate all three velocity components at two streamwise positions simultaneously: one at the tip of the shifted array, and the other in the plane of the four other arrays via interpolation of the four values obtained from these four arrays. A probe of this type was used in a field experiment (Kholmyansky *et al.* 2001*b*; Galanti *et al.* 2003) where spatial derivatives, based on the Taylor hypothesis, were compared with those measured directly. Moreover, it became possible to obtain estimates of the full (Lagrangian) acceleration and its (Eulerian) 'components', $\boldsymbol{a}_l = \partial \boldsymbol{u}/\partial t$ and $\boldsymbol{a}_c = (\boldsymbol{u} \cdot \nabla)\boldsymbol{u}$.

A further important step was the attachment to the probe of cold wires for temperature measurements. Each array was completed with a separate cold wire thus forming a 25-wire probe. In addition to three velocity components, nine components of the spatial velocity gradient tensor and three components of temporal velocity derivatives, the new probe can also measure temperature, three components of temperature gradient and a temporal derivative of temperature (all without invoking the Taylor hypothesis).

At this first stage the cold wires were of the same diameter as the hot wires, namely 2.5 μm, therefore the frequency bandwidth of the temperature measurements was less than that for the velocities: while the channels of the anemometer had a flat frequency response in the band of about 4 kHz, for the thermometers such a band lasted only unfil about 300 Hz. We plan to manufacture probes with thinner wires for further experiments.

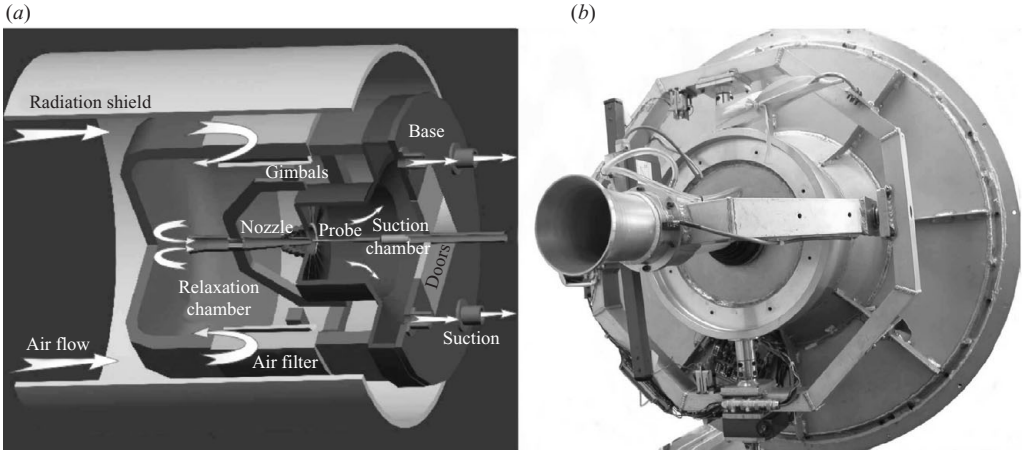

FIGURE 2. The calibration unit. (*a*) Schematic. (*b*) Interior (container removed).

Incorporation of cold wires into a probe required special efforts to minimize the effects of their heating by the hot wires. Though the cold wires are very close to the hot wires of the corresponding array (about 0.2 mm ahead from its tip), no direct heating of the cold wires was observed, even at very low flow velocities. But the prongs, supporting the cold wires, were heated and transferred this heat to the wires through thermal conduction. This problem was solved by shaping the cold-wire prongs so that they were far enough from the hot-wires with their prongs in the vicinity of the tip of the probe (figure 1*a*, *b*).

The described solution did not prevent the heating of the cold-wire prongs, it only drastically decreased the heat transfer from the prongs to the cold wires. But the varying heating and cooling (by the flow) of the prongs resulted in variations of their temperature and therefore resistance. The resistance of the prongs was measured by the thermometer together with that of the cold wires. If not constant, it caused errors in the temperature data.

In order to reduce such errors to a tolerable value we replaced the tungsten prongs by manganin: the temperature coefficient of the electrical resistance of manganin is 400 times smaller than that of tungsten. The hot-wire prongs in the new probes were also made of manganin. Such probes were used in the reported experiments. An additional advantage was the improvement of their life span.

2.2. *Calibration*

The calibration of the multi-wire probe consists of two main steps:

(i) obtaining calibration data, using the calibration unit, data acquisition equipment and software (field calibration);

(ii) processing the calibration data to calculate calibration coefficients.

Calibration coefficients are used to transform the voltages recorded in the measurement runs into physical values, in our case components of the velocity vector.

The function of the calibration unit (figure 2) is to place the probe in a flow with velocity of known and variable value at various angles with respect to two orthogonal axes. Resistances of hot wires are low, therefore small changes of contact resistance in connectors may affect the calibration characteristics and produce errors in measured velocity values. Such errors are especially dangerous because these velocity values, taken at close points within a probe, are used to calculate velocity differences and

space derivatives, and even small errors in measured velocities may result in high errors of the differences. To avoid errors of this kind, the calibration must be performed with the probe connected to its cable in its working position.

Figure 2(*a*) shows the flow in our calibration unit. The flow is produced by suction, therefore we avoid its heating by pumping. The calibration flow is a jet formed by a nozzle. When suction is on, the atmospheric air enters the container through a filter, covering openings in its sidewall. From there, the air enters the jet unit which consists of a contractor, a honeycomb and a nozzle. The flow passing through these elements forms a jet with uniform velocity profile around its axis and a low level of fluctuations. The outlet of the nozzle, where the tip of the probe is located, opens to a suction chamber.

In order to allow three-dimensional calibration, the jet unit can be rotated around two orthogonal axes: it is mounted on a high-precision gimbals mechanism. The rotation of the gimbals is performed by two similar units, each including a motor, a gear assembly and a synchronous resolver that serves for the measurement of the angle of rotation.

The value of the velocity magnitude in the jet is obtained by measuring pressure difference at two cross-sections of the nozzle using an electronic differential manometer. The velocity can be calculated using Venturi's formula.

The field calibration is controlled by a computer program. Usually it is performed at 49 angular positions within a spatial angle of up to 35°. At each position, the calibration data are taken at ten velocities within a specified range. Therefore the calibration data contain 490 samples. The duration of such a calibration is about 10 min. The sample consists of the values of velocity magnitude, two angles, twenty readings of the hot-wire channels and five readings of the thermometer channels.

The field calibration also includes a simple step of determining the sensitivity of the thermometer channels: a preset jump in the bridge resistance is activated, and the thermometer outputs are recorded before the jump and after it. Thus, we obtain the gain of the channels. Knowing the resistance of the cold wires at certain temperature and the temperature coefficient of the electrical resistance of their material (tungsten), we can calculate the sensitivity.

Simultaneous temperature data, recorded during the calibration and the measurement run, make it possible to implement a correction of hot-wire data distorted by temperature variations. The output of the hot-wire channel depends on the temperature of the flow, and this dependence is approximated well by a linear function. Though the flow temperature fluctuations are small relative to the temperature of the hot wires (which is of the order of 200 °C), even small errors in the velocity values, correlated with temperature, can distort the joint velocity–temperature statistics. Therefore the correction is important.

We measure the coefficient in the linear function mentioned above (separately for each hot-wire channel). A small heating element is installed in the jet unit of the calibration device. At the final stage of the field calibration, the heating element is activated several times for a short period of time, thus producing a series of heat pulses. The outputs of the hot- and cold-wire channels are recorded during each pulse. The coefficients in question can be found from linear regression of each hot-wire channel on the corresponding cold-wire one.

The processing of the calibration data to calculate calibration coefficients is performed by least-squares approximation of the calibration data by multidimensional polynomials of the Chebyshev type.

The space derivatives in the lateral and vertical direction were calculated using the differences of the velocity values from the corresponding pair of arrays (excluding the central one), divided by their separation. The longitudinal derivatives were calculated using the time differences (Taylor hypothesis) and also using true space differences, as described above.

2.2.1. *Jet facility*

The calibration unit, in addition to its direct function, is used as a main part of a jet facility. This facility is built for performing laboratory experiments in turbulent jet flow, including those in a slightly heated jet. The measurements started recently and we have only some preliminary results that will be reported in Part 3.

2.3. *Performance and other tests of the system*

One of the difficulties in using multi-hot-wire systems is the complexity of estimation of errors, mostly coming from the calibration process when full three-dimensional calibration is employed. These errors should be distinguished from the instrumental noise, which in our case was relatively small as compared to the calibration errors. The complexity of such estimation comes not only from the nonlinear nature of the hot-wire anemometer, but also and mainly from the existence of singularities in the function, approximating the calibration data. Though this is known in the literature dedicated to multi-wire calibration, it was not analysed mathematically in a rigorous manner. B. Youssin (unpublished work) made a rigorous mathematical analysis of an idealized probe (geometrical identity of the wires, King law). The main point is that since the individual wires sense mostly the velocity, normal to them, the relations between the anemometer outputs and velocity components are not invertible when the angle, γ, between the instantaneous velocity vector and the probe axis exceeds some value around 35°. It was found that there was a strong dependence of the calibration errors on this angle and fast growth of the errors when the velocity vector approaches the singular points, located somewhere outside the cone with half-width of 35°. This was one of the reasons for using the Sils-Maria site where the range of γ was much smaller.

The complexity, mentioned above, led us to follow the approach described in § 2 of Tsinober *et al.* (1992), where a series of checks was undertaken in order to evaluate the performance of the system with some emphasis on the multi-hot-wire probe performance. These and extra checks were made in our later works (Kholmyansky & Tsinober 2000; Kholmyansky *et al.* 2000, 2001*a*, *b*; Galanti *et al.* 2003, 2004). As well as the checks made in Tsinober *et al.* (1992) and in later papers, we have made a number of additional ones. We will mention the main former checks briefly, and the additional checks in more detail below.

(*a*) Check of the raw data. For each of the twenty hot-wire signals (and five cold-wire ones) histograms were plotted. Each point located outside the main bell of the histogram was inspected. In many cases such points were sharp jumps out of a smooth curve of the signal. The jumps could be caused by a particle or a water drop hitting the wire and were corrected by interpolation. A similar check was then performed for the differences between the sequential points that permitted further elimination of artificial jumps in the signal.

(*b*) Check of the velocity data. Each velocity component from each array was similarly inspected for jumps (caused by the same reasons, but not detected by the check of the raw data) and corrected by interpolation when necessary. Then for each array, angles, γ, between the instantaneous velocity vector and the axis of the

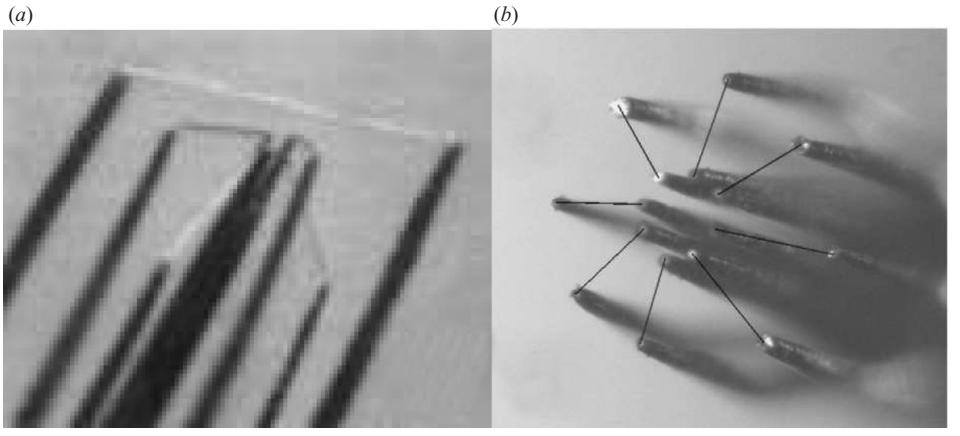

FIGURE 3. Two 'in one point' probes. (*a*) A four-wire and a single-wire probe; (*b*) two four-wire probes.

probe were calculated. Sometimes run segments were detected where the values of γ exceeded the calibration range ($\pm 35^\circ$) and therefore came close to the singular points. Such segments were excluded from further processing.

(*c*) Criteria for the run evaluation. Several criteria were applied to evaluate the quality of each run.

(i) Approximation errors. The program, calculating the calibration coefficients, calculates and prints the value of χ^2, characterizing the quality of the approximation. We use the estimate of the error as $(\chi^2/N)^{1/2}$, where N is the number of calibration points. Though this estimate is rough and relates to the whole run, we know that when its values reach tens of cm s^{-1}, further processing is not worth while.

(ii) The scatter of the mean and the root mean square (RMS) values of the velocity components from various arrays.

(iii) The ratio of the variances of the velocity derivatives, $\partial u_j/\partial x_k$, to that of $\partial u_1/\partial x_1$ in comparison with the values for isotropy. Though one cannot claim perfect isotropy (even local) and should not rely on it, still very high deviations point to poor data rather than to anisotropy.

(iv) An important check is the one based on the continuity equation. Namely, for $A = \partial u_1/\partial x_1$ and $B = -\partial u_2/\partial x_2 - \partial u_3/\partial x_3$ the correlation coefficient between A and B is a sensitive indicator of the quality of the data. Theoretically it should be 1, but in the best measurements known it does not exceed 0.6–0.7. Much lower values point to a problematic run. In the present experiments, this correlation coefficient was typically better.

(*d*) Data selection. Even when all the above-mentioned checks show a reasonable quality of run, some quantities, most sensitive to the calibration errors, show good results only after the selection of samples corresponding to a relative divergence of less than 0.1. The example is the tear-drop plot shown in figure 11.

(*e*) A special check was made with 'two probes in one point' initiated in Tsinober *et al.* (1992). The check consisted of comparing a four-wire array with a single wire (put in 'one point' as shown in figure 3*a*, and described in more detail in Tsinober *et al.* 1992). The main result is that the correlation coefficient between the streamwise velocity fluctuations measured by the two is very close to 0.99. This result is important not only as evidence of performance of the four-wire array, but also of the calibration procedure.

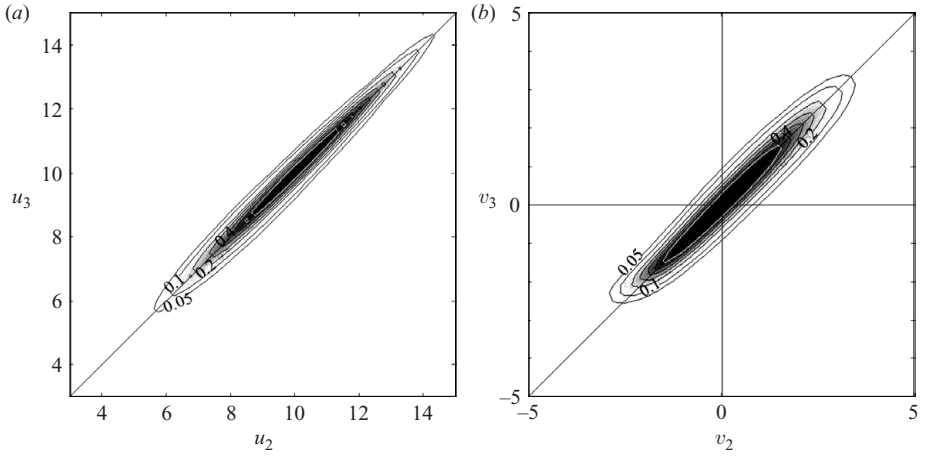

FIGURE 4. Joint PDFs of streamwise (*a*) and transverse (*b*) components from two 'in one point' four-wire probes. (*a*) Correlation coefficient = 0.983; (*b*) 0.957.

A more elaborate and new check was made with two four-wire arrays again put in 'one point' as shown in figure 3*b* (Tsimanis 2005). The correlation coefficient in this check was over 0.98 for the streamwise velocity fluctuations and 0.96 for the transverse velocity fluctuations measured by the two probes. We show also two examples of the corresponding joint probability density functions (PDFs) (figure 4). Both measurements were made using the probe with the scale at the tip about 1.5 mm (in our field experiment each array was less than 0.9 mm at the tip) in the region of the largest mean velocity gradient in our jet facility mentioned above.

(*f*) We had the opportunity to make an overall check, giving an indication of the performance of our system. In the course of an experiment, performed in the low-noise wind tunnel in the Aeronautics Department, Imperial College, London, we found that the RMS values of the velocity components from each of five four-wire arrays did not exceed 0.12 %. This is only slightly higher than the known *a priori* level of turbulence in the wind tunnel, estimated as 0.1 %.

2.4. *Equipment*

The general layout of the experimental equipment is shown in figure 5(*a*), and a photograph of the instrument rack in figure 5(*b*).

2.4.1. *Anemometer channels*

The hot-wire anemometer channel is a standard device. We used a new 20-channel constant-temperature anemometer (2 in figure 5*b*), specially designed and manufactured for us. Its main feature is a symmetric bridge. In most cases, three arms of the bridge are located in the anemometer itself, and the appropriate hot wire of the probe is connected to the bridge by a cable. The cable introduces asymmetry (mainly inductive) into the bridge that is proportional to the length of the cable. In order to prevent the excitation of oscillations in the circuit, it is necessary to limit the length of the cable. In the field experiment, we have to work with relatively long cables, and the circuit stability was reached by individual fitting of compensating impedances in each channel.

In the new device only two arms of the bridge are internal. The other two (a hot-wire of the probe and a constant resistor) are located outside, close to each other. They are connected to the rest of the bridge symmetrically, by a shielded twisted-pair

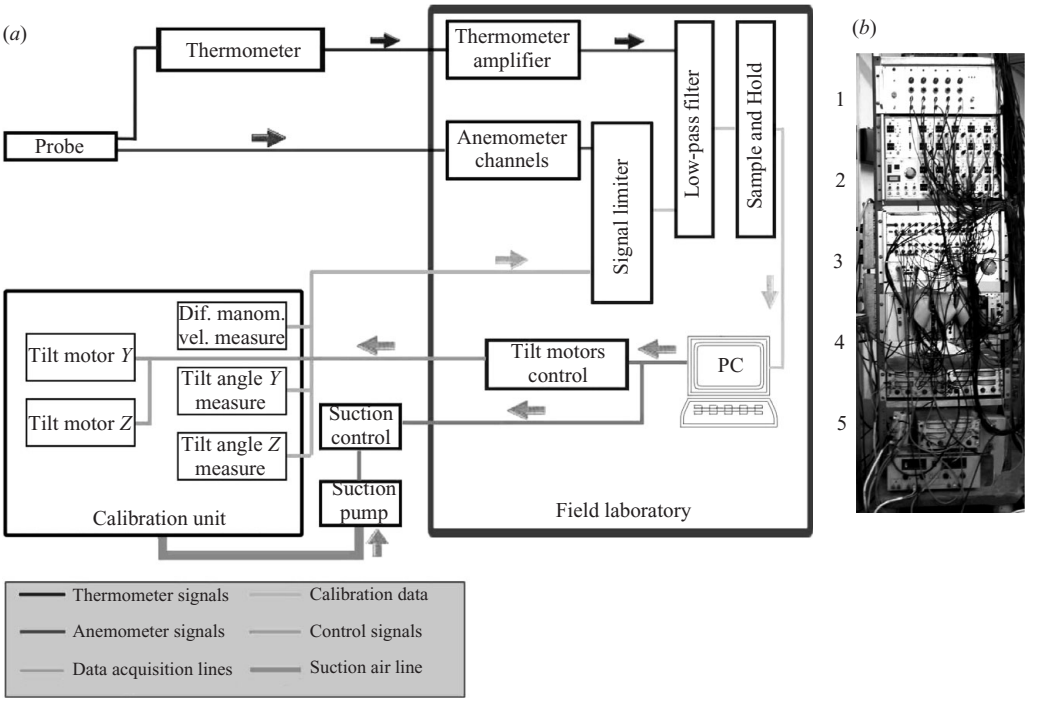

FIGURE 5. The experimental equipment layout. (*a*) Chart of signal connections. (*b*) Instrument rack: 1, thermometer amplifier; 2, anemometer channels; 3, signal limiter; 4, low-pass filters and 'sample and hold'; 5, power supply blocks.

cable. The new anemometer worked with 20 m cable without compensating circuitry and showed good performance.

2.4.2. *Five-channel thermometer*

The thermometer was also specially designed and manufactured for our experiments. It consists of two blocks: the bridge and preamplifier block (Thermometer in figure 5*a*) is located not far from the probe, and the thermometer amplifier (figure 5*a* and 1 in figure 5*b*) is in the field laboratory.

2.4.3. *Data acquisition*

In the course of a measurement run or field calibration, all relevant signals are recorded onto a PC hard disk. The main component of our data acquisition system is an input–output PC card (PCI-MIO-16E-1 from National Instruments^{TM}), supplemented with an SCXI chassis and modules (4 in figure 5*b*). We use low-pass filters and 'sample and hold' modules. The filters (with cutoff frequency set at 4 kHz) are used as an anti-aliasing device. The 'sample and hold' modules provide for simultaneous sampling of all the channels, an important feature in multi-channel systems. The signal limiter (3 in figure 5*b*) is an auxiliary device preventing saturation of all the channels of the data acquisition system in the case when one or more signals are far out-of-scale (this can happen, for instance, if some wires are broken.) Any signal within the scale passes this device unaffected. Any out-of-scale signal, entering the device, exits with the value of the corresponding scale limit.

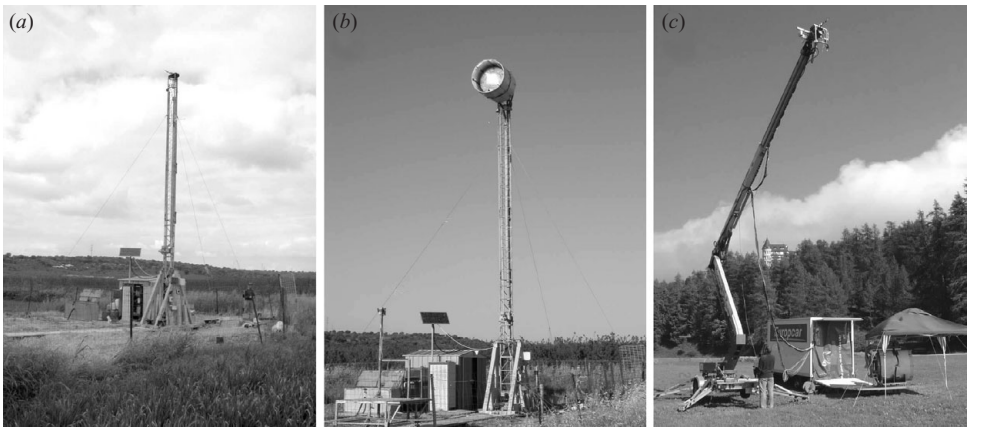

FIGURE 6. The experimental sites. (*a*) Kfar Glikson, Israel, measurement position. (*b*) Kfar Glikson, calibration position. (*c*) Sils-Maria, Switzerland.

2.5. *Sites*

The choice of sites was a complicated problem. The site must be reasonably flat and homogeneous, at least in the direction of the dominating winds. Naturally, it must satisfy certain logistic requirements.

Most of our preparatory work and first experiments were performed at the measurement station that we erected in a field at the Kfar Glikson kibbutz, few kilometres to the north-east of Pardes-Hanna, Israel (figure 6*a*, *b*). The site is rather flat in the west-south-west direction, about 10 km from the sea shore, and the winds from there are suitable for the experiments.

The site is equipped with a specially designed mast. It is of a balanced boom crane configuration. The main boom of the mast can be rotated on the bearings around a horizontal axis, positioned 2 m above the ground. The mast has a low vibration level and permits convenient mounting of the probe and the calibration unit. The probe is fixed on top of the mast. In order to perform a measurement run, we lift the mast with the probe, exposed to the wind (see figure 6*a*). To calibrate, we lower the mast, attach the calibration unit to its boom so that the tip of the probe is at the centre of the nozzle outlet, and then lift the mast with the calibration unit (see figure 6*b*).

In August–September 2004, we performed a field experiment at another site, located in Switzerland, on the outskirts of the village of Sils-Maria, about 1800 m above sea level. The site is a rather flat valley of more than 1 km width, surrounded by two parallel mountain ridges. It is famous for the so-called Maloja wind (a regular strong orographic wind, blowing along the valley from the village of Maloja towards Sils-Maria).

A preliminary experiment at this site was carried out in August 2003 to obtain rough estimates of the characteristics of the Maloja wind, mainly the stability of its direction in the mean and the range of the direction fluctuations. Here we provide a short account, more details are given in Report (2003). The measuring instrument was a three-component sonic anemometer that gave short (5 min) records of wind velocity components as well as the temperature of the air. All the values were produced with a space averaging over the base of the instrument (about 10 cm) at a sampling rate of 100 Hz. The records were made at several heights above the ground ranging from 0.85 to 3.6 m.

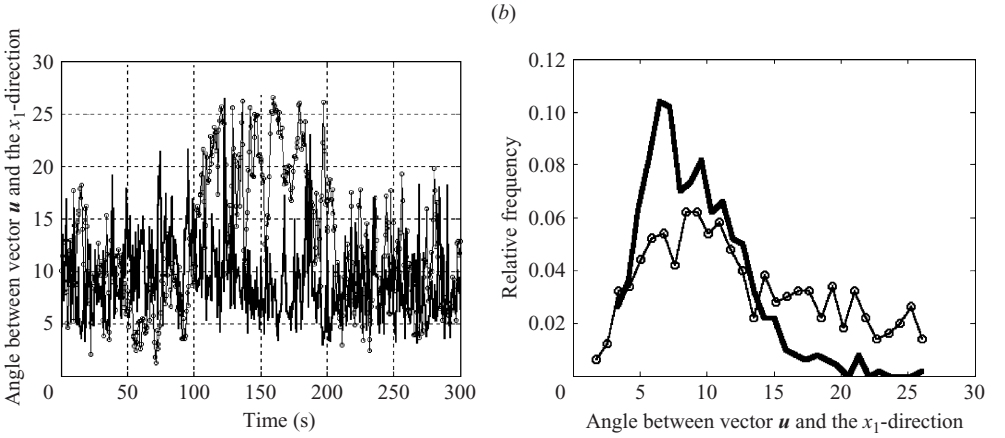

FIGURE 7. (*a*) Time series of the total angle between the velocity vector, $\boldsymbol{u}$, and the axis x_1-direction and (*b*) the corresponding relative frequencies plot. —, Sils-Maria data 25 August 2003; —•—, Kfar Glikson data.

The preliminary experiment confirmed the expectation that the Sils-Maria site was a good location for the micro-turbulent measurements. As an example we show (figure 7) the comparison of the total angle between the velocity vector, $\boldsymbol{u}$, and the axis x_1-direction for the data from Kfar Glikson and Sils-Maria. The behaviour of this angle is of the utmost importance: the precision of the velocity values obtained with the help of the calibration data, as described above, is higher when this angle is small. The precision is poor if the total angle is higher than the calibration range of 35°. The Sils-Maria data are strongly concentrated within a small angle and, in practice, do not reach the dangerously high values. The Kfar Glikson data, on the contrary, cover a wide band of angles, and there is a probability of exceeding the value of 35°.

The main experiment at the Sils-Maria site was performed in a configuration similar to that of the Kfar Glikson experiments. For the first time the full probe, with the central array shifted forward and containing also cold wires, was used in the field. It was not reasonable to bring our mast there or to build a similar one. Instead a lifting machine was used (figure 6*c*). The cradle of the lifting machine was removed, and a special interface was designed and manufactured, permitting us to fix the probe and the calibration unit to the lifting machine in the same way as they were fixed to the mast.

2.6. *Profile measurements*

Besides the equipment for microscale turbulent measurements, described above, we used at the Sils-Maria site an independent system for measurement of vertical profiles of wind velocity and temperature in a range of heights from 0.5 to 11.5 m. There were six fixed stations in this range. A single set of measuring instruments was used: a sensitive cup anemometer and a resistance thermometer with suction and radiation protection. This set was mounted on a carriage, rolling up and down along a special mast, erected at the distance of about 30 m from the lifting machine. A controller (specially designed for the system) moved the carriage up the mast. At each station the movement stopped, and after a pause (to let the readings reach the steady state) the values were measured and saved to a data logger. From the top station the carriage returned to the lowest one, and the cycle repeated.

Height m	U_1 m s^{-1}	u_1' m s^{-1}	u_2' m s^{-1}	u_3' m s^{-1}	λ m	$\eta \times 10^3$ m	r_{uw}	C	$Re_\lambda \times 10^{-3}$
0.8	5.6	1.25	0.93	0.59	0.025	0.35	−0.34	0.56	1.6
1.2	5.6	1.05	0.89	0.54	0.032	0.43	−0.29	0.51	1.8
2.0	6.7	1.23	0.84	0.53	0.057	0.46	−0.34	0.59	3.7
3.0	6.8	1.12	0.84	0.62	0.059	0.53	−0.32	0.55	3.4
4.5	7.5	1.22	1.18	0.63	0.090	0.60	−0.35	0.64	5.8
7.0	7.5	1.04	1.04	0.62	0.096	0.63	−0.39	0.51	5.3
10.0	8.0	1.06	0.90	0.61	0.119	0.76	−0.36	0.59	6.6

TABLE 1. Basic information on the experimental runs. The notation is as follows: x_1, horizontal streamwise; x_2, horizontal spanwise; and x_3, vertical coordinates; u_i, corresponding components of velocity fluctuations; u_i', their *rms* values; $\lambda = u_1'/rms(\partial u_1/\partial x_1)$, Taylor microscale; $r_{uw} = \langle u_1 u_3 \rangle / \sigma_{u_1} \sigma_{u_3}$, correlation coefficient between the streamwise and vertical components of velocity fluctuations; C, Kolmogorov constant from the power spectrum of u_1 in the inertial range: $E_1^{u_1}(k) = C\langle\epsilon\rangle^{2/3} k^{-5/3}$, where ϵ – is a dissipation rate.

The profiles obtained show the background conditions of the runs, they are also used for estimates of mean vorticity and strain (see § 3.1).

3. Some general results

Though the emphasis of the present project (described in Parts 2 and 3) was on accelerations and temperature, we present a number of results, similar to those published previously (Kholmyansky & Tsinober 2000; Kholmyansky *et al.* 2000, 2001*a*, *b*; Galanti *et al.* 2003, 2004), with the focus on the quantities associated with velocity derivatives. The main aim is to demonstrate similarities and differences along with important additional information. The basic data on representative runs for several heights are presented in tables 1 and 2. The thermal stability at the site, when our measurements were performed, is discussed in Part 3 § 4.1. It can be described as slight instability.

The skewness of the derivatives $\partial u_2/\partial x_2$ and $\partial u_3/\partial x_3$ does not differ more than twice from that of $\partial u_1/\partial x_1$. Still, this difference is rather high, probably because of the known difficulties in obtaining odd moments (see the scatter of the data in figure 8 from Sreenivasan & Antonia 1997) and the additional difficulty in obtaining transverse velocity derivatives. Also, noteworthy is the agreement of these values and those of the flatness with the values known from literature (e.g. see the review by Sreenivasan & Antonia (1997) and figure 8). Slight deviation of some of our points for the flatness from the bulk of the data can probably be explained by a certain under-resolution of the velocity derivatives.

3.1. *RDT-terms*

As mentioned, our main interest was in the field of derivatives of velocity fluctuations, $\partial u_i/\partial x_j$. However, in order to limit ourselves to the study of this field only, it was necessary to estimate the influence of the processes, associated with the mean flow gradient, $\mathrm{d}U_1/\mathrm{d}x_3$, on production of $\partial u_i/\partial x_j$, i.e. production of enstrophy, ω^2, and magnitude of strain, s^2. Well-known order-of-magnitude estimates (Tennekes & Lumley 1972) show that at high Reynolds numbers, production of enstrophy, $\langle\omega^2\rangle/2$, is mainly associated with the term $\langle\omega_i\omega_k s_{ik}\rangle$, i.e. with the self-amplification of the field of vorticity/strain fluctuations. According to these estimates, the contributions to the enstrophy production, associated with the mean velocity gradient, $\langle u_k\omega_i\rangle\partial\Omega_i/\partial x_k$,

Skewness	Height (m)	$\frac{\partial u_1}{\partial x_1}$	$\frac{\partial u_2}{\partial x_2}$	$\frac{\partial u_3}{\partial x_3}$	$\frac{\partial u_i}{\partial x_k},\ i \neq k$	$\frac{\langle \omega_i \omega_k s_{ik} \rangle}{\langle \omega^2 \rangle \langle s^2 \rangle^{1/2}}$	$-\frac{\langle s_{ij} s_{jk} s_{ki} \rangle}{\langle s^2 \rangle^{3/2}}$
Measured	0.8	−0.46	−0.35	−0.29	0.01–0.14	0.16	0.23
Estimated						0.52	0.45
Measured	1.2	−0.64	−0.38	−0.22	0.03–0.15	0.19	0.26
Estimated						0.69	0.63
Measured	2.0	−0.54	−0.34	−0.36	−0.12–0.20	0.18	0.27
Estimated						0.61	0.57
Measured	3.0	−0.64	−0.43	−0.55	−0.11–0.08	0.20	0.29
Estimated						0.44	0.45
Measured	4.5	−0.51	−0.45	−0.25	−0.18–0.09	0.20	0.28
Estimated						0.67	0.64
Measured	7.0	−0.56	−0.42	−0.54	−0.02–0.25	0.20	0.36
Estimated						0.38	0.40
Measured	10.0	−0.68	−0.35	−0.44	−0.21–0.22	0.21	0.43
Estimated						0.39	0.44
Flatness		$\frac{\partial u_i}{\partial x_k}$	$\frac{15}{7}\frac{\langle s^4 \rangle}{\langle s^2 \rangle^2}$	$\frac{9}{5}\frac{\langle \omega^4 \rangle}{\langle \omega^2 \rangle^2}$	$\frac{\langle \omega^2 s^2 \rangle}{\langle \omega^2 \rangle \langle s^2 \rangle}$	$3\frac{\langle (\omega_k s_{ik})^2 \rangle}{\langle \omega^2 \rangle \langle s^2 \rangle}$	
Measured	0.8	5.0–13	10.5	11.2	3.2	2.0	
	1.2	5.5–24	21	16	6.0	5.1	
	2.0	5.6–12	19	56	9.8	5.7	
	3.0	8.6–15	11	19	4.3	2.3	
	4.5	8.0–65	20	19	6.1	3.8	
	7.0	7.3–18	16	21	5.8	2.8	
	10.0	14.5–33	18	26	6.9	3.3	
Gaussian		3	3	3	1	1	

TABLE 2. Skewness and flatness (kurtosis) values of velocity derivatives. The row marked 'Estimated' in the table for skewness contains values of $\langle \omega_i \omega_k s_{ik} \rangle / \langle \omega^2 \rangle \langle s^2 \rangle^{1/2}$ and $\langle s_{ij} s_{jk} s_{ki} \rangle / \langle s^2 \rangle^{3/2}$, that were obtained assuming the isotropic relations $\langle \omega_i \omega_k s_{ik} \rangle = -17.5 \langle (\partial u_1 / \partial x_1)^3 \rangle$ and $\langle s_{ij} s_{jk} s_{ki} \rangle = (105/8) \langle (\partial u_1 / \partial x_1)^3 \rangle$.

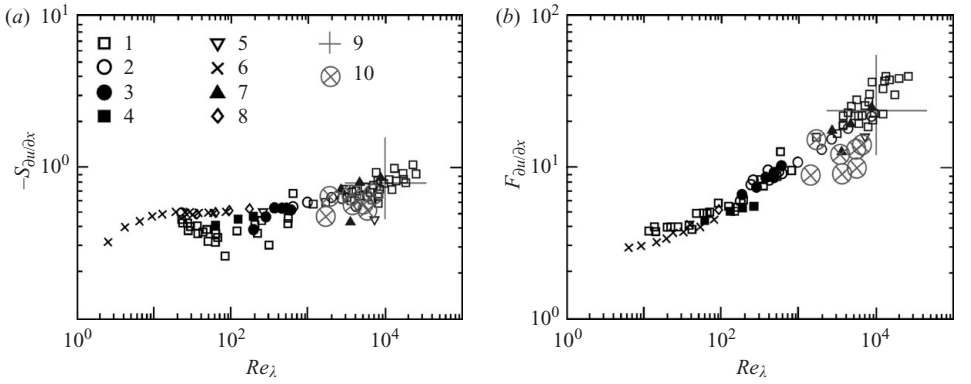

FIGURE 8. (*a*) Skewness and (*b*) flatness of the velocity derivatives. The plots are from the review by Sreenivasan & Antonia (1997) with our results added. 1, Van Atta & Antonia (1980); 2, Antonia & Chambers (1980); 3–5, Sreenivasan & Antonia (1997): 3, plane jet, 4, wake, 5, atmospheric boundary layer; 6, Kerr (1985); 7, Gibson, Stegen & Williams (1970); 8, Jimenes *et al.* (1993); 9, Kholmyansky *et al.* (2001*a*); 10, present work.

Height (m)	0.8	1.2	2.0	3.0	4.5	7.0	10.0
Max ratio	0.003	0.003	0.001	0.002	0.0003	0.0003	0.0002

TABLE 3. Maximum absolute values of the ratio of the terms, associated with the mean flow gradient, to the main production terms, $\langle \omega_i \omega_k s_{ik} \rangle$ and $-\langle s_{ij} s_{jk} s_{ki} \rangle$.

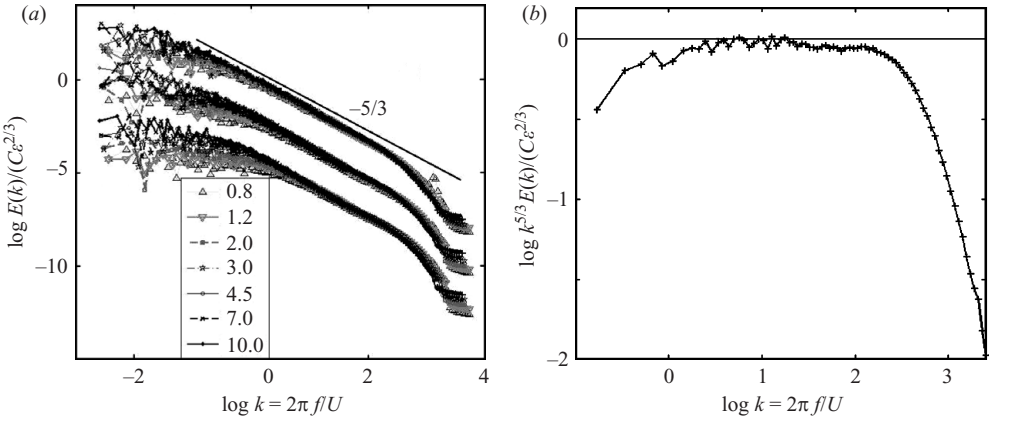

FIGURE 9. (*a*) Normalized power spectra of the three velocity components at various heights. The spectra of u_2 are shifted by –2 and of u_3 by –4. (*b*) Example of compensated power spectrum (component u_1, height 1.2 m.)

$\langle \omega_i \omega_k \rangle S_{ik}$, $\Omega_k \langle \omega_i s_{ik} \rangle$, i.e. owing to the presence of mean vorticity, Ω_i, and strain, S_{ij}, are small compared to $\langle \omega_i \omega_k s_{ik} \rangle$. Similar estimates remain valid for the production of the total mean squared strain, $\langle s^2 \rangle / 2 \equiv \langle s_{ij} s_{ij} \rangle / 2$. Namely, its production is mainly due to the term $-\langle s_{ij} s_{jk} s_{ki} \rangle$, whereas the contributions to the strain production, associated with the mean velocity gradient, $-\langle u_k s_{ij} \rangle \partial S_{ij} / \partial x_k$ and $\langle s_{ij} s_{ik} \rangle S_{kj}$, are small compared to $-\langle s_{ij} s_{jk} s_{ki} \rangle$. Our present experiments (see also Kholmyansky *et al.* 2001*a*) showed that this is really the case (see table 3).

It is noteworthy that such 'smallness' of these RDT-like terms is observed in a turbulent channel flow at a rather moderate Reynolds number too (Sandham & Tsinober 2000). Another related result is the smallness of terms, associated with forcing, in the equations for vorticity and strain (Galanti & Tsinober 2000).

3.2. *Velocity*

A broad $-5/3$ range was observed for the power spectra of the three velocity components (figure 9*a*) at all heights with about four decades of magnitude at the lower height of 0.8 m and about six decades at the largest height of 10 m for the component u_1. Similar observations were made for the temperature fluctuations. At the low end of the wave-number scale, with the decrease of the height, the spectra of u_2 deviate faster from the $-5/3$ law than those of u_1. The spectra of u_3 deviate even faster.

The compensated spectra do not look 'nice' (figure 9*b*), so the inertial range is considerably shorter. Similar behaviour is observed when looking at the r-dependence of structure functions (with the exception of Kolmogorov's $-4/5$ law, Kolmogorov (1941*b*), for the third-order velocity structure function and the $-4/3$ Yaglom's law for the corresponding mixed velocity–temperature structure function, Yaglom 1949).

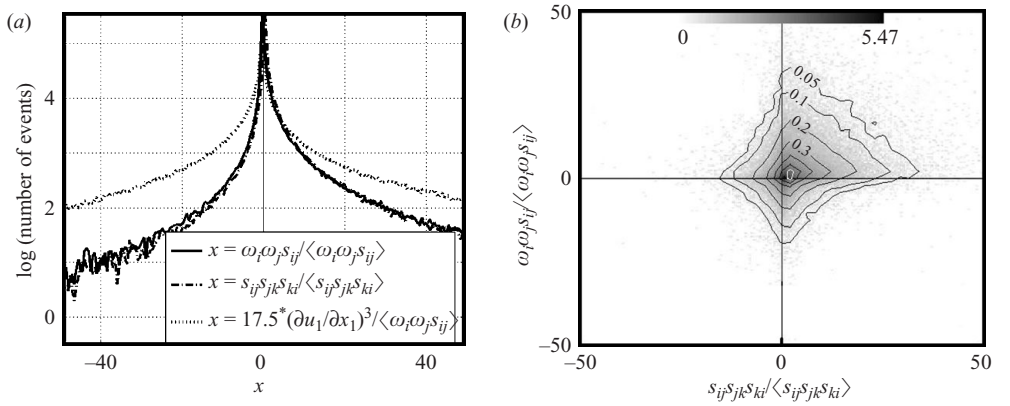

FIGURE 10. (*a*) PDFs of $\omega_i\omega_j s_{ij}$, $-(4/3)s_{ij}s_{jk}s_{ki}$ and their surrogate, $-17.5(\partial u_1/\partial x_1)^3$ and (*b*) joint PDF of $\omega_i\omega_j s_{ij}$ and $-(4/3)s_{ij}s_{jk}s_{ki}$. (*b*) Correlation coefficient = 0.265. Density shows log (number) of points.

All this seems to be related to a much broader issue concerning the very existence of scaling in turbulent flows.

3.3. *Velocity derivatives*

As mentioned, one of the main objectives of our present work is the field of velocity derivatives. In the following, we show a number of key properties studied previously in our field experiments and some new ones. Some basic results are shown in table 2.

3.3.1. *Enstrophy and strain production*

Production of enstrophy, ω^2, and strain, s^2, are among the basic processes in turbulent flows. The PDFs of production of enstrophy, $\omega_i\omega_j s_{ij}$, and strain, $-(4/3)s_{ij}s_{jk}s_{ki}$, as well as one of their surrogates, $-17.5(\partial u_1/\partial x_1)^3$, are shown in figure 10(*a*). Their positively skewed nature is seen quite clearly. The coefficients are chosen equal to those appearing in the relations for homogeneous ($-4/3$) and isotropic (-17.5) flow. As observed previously, the PDF of the surrogate $-17.5(\partial u_1/\partial x_1)^3$ is considerably different. This is true also of other surrogates, such as the most popular dissipation surrogate $15(\partial u_1/\partial x_1)^2$.

Though the univariate PDFs of $\omega_i\omega_j s_{ij}$ and $-(4/3)s_{ij}s_{jk}s_{ki}$ look similar, the point-wise relation between $\omega_i\omega_j s_{ij}$ and $-(4/3)s_{ij}s_{jk}s_{ki}$ is strongly non-local owing to the non-local relation between vorticity and strain. Consequently, locally they are very different as can be seen from their joint PDF (figure 10*b*): they are only weakly correlated and there are many points with small $\omega_i\omega_j s_{ij}$ and large $-(4/3)s_{ij}s_{jk}s_{ki}$ and vice versa. The correlation coefficient between $\omega_i\omega_j s_{ij}$ and $-(4/3)s_{ij}s_{jk}s_{ki}$ is of the order of 0.25. Their rates, i.e. $\omega_i\omega_j s_{ij}/\omega^2$ and $-(4/3)s_{ij}s_{jk}s_{ki}/s^2$, are correlated even less.

Among the qualitative universal features of most (at least) turbulent flows there is a so-called 'tear-drop' feature observed in the invariant map of the second invariant, $Q = (\omega^2 - 2s_{ik}s_{ik})/4$, versus the third invariant, $R = -(s_{ik}s_{km}s_{mi} + (3/4)\omega_i\omega_k s_{ik})/3$, of the velocity gradient tensor, $\partial u_i/\partial x_k$. This feature was observed in all our runs. Two examples are shown in figure 11.

An important point is that figure 11(*a*) was plotted for the subset of points (about 6 % of the whole set), selected by the criterion of relative velocity divergence smaller than 0.1, as done in another context by Lüthi, Tsinober & Kinzelbach (2005). The

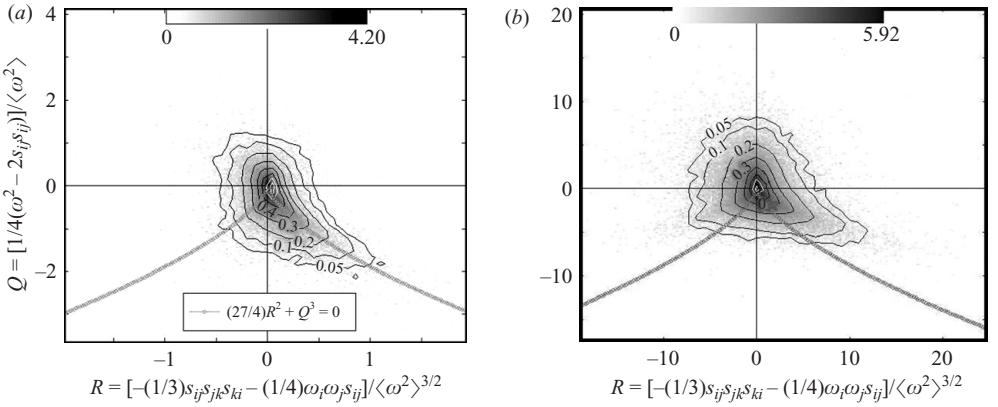

FIGURE 11. Joint PDF of the second invariant, $Q = (\omega^2 - 2s_{ik}s_{ik})/4$, and the third invariant, $R = -(s_{ik}s_{km}s_{mi} + (3/4)\omega_i\omega_k s_{ik})/3$, of the velocity gradient tensor. (*a*) Selected data and (*b*) full data set. (*a*) Correlation coefficient −0.429; (*b*) −0.274.

	$\omega_i\omega_k s_{ik}$	$\omega_i\omega_k s_{ik}/\omega^2$	$-s_{ij}s_{jk}s_{ki}$	$-s_{ij}s_{jk}s_{ki}/s^2$
ω^2	0.36	0.13	0.14	0.10
s^2	0.30	0.23	0.38	0.28

TABLE 4. An example of correlation coefficients between production terms versus enstrophy and strain, height 3 m.

$R - Q$ plot belongs to the kind of statistical properties which are strongly sensitive to errors. For the whole set of data (see figure 11*b*), this plot resembles the one for a Gaussian velocity field, which is symmetric with respect to the vertical axis (Chertkov, Pumir & Shraiman 1999). The left 'horn' in this plot is more pronounced because of the larger level of noise. Statistics of all the quantities reported in the paper are not sensitive to the above selection procedure, with the exception of the $R - Q$ plot. We do not have a definite explanation of this behaviour, neither have we found (so far) other quantities with such sensitivity. One of the possibilities is that quantities which are flux-like (i.e. they are of the form div$\{\ldots\}$ as R and Q are) exhibit such a property. This is a matter for further study which is now under way.

Another kind of relation of interest is the one between the quantities responsible for enstrophy and strain production and enstrophy and strain themselves. The corresponding correlation coefficients are shown in table 4.

The main feature is that strain production and its rate are much less correlated with enstrophy than with strain, whereas enstrophy production is equally correlated with both, but its rate is more correlated with strain. Recall that the particular interest in the strain production is because dissipation is directly related to strain rather than enstrophy. It was, therefore, stressed (Tsinober 1998*a*, *b*, 2001; Tsinober, Ortenberg & Shtilman 1999 and references therein) that the cascade, whatever this means, is associated with strain production rather than with vortex stretching and enstrophy production. Moreover, enstrophy production (and vortex stretching) opposes the production of strain/dissipation. This is closely related to the issue of reduction of nonlinearity, which is our next concern.

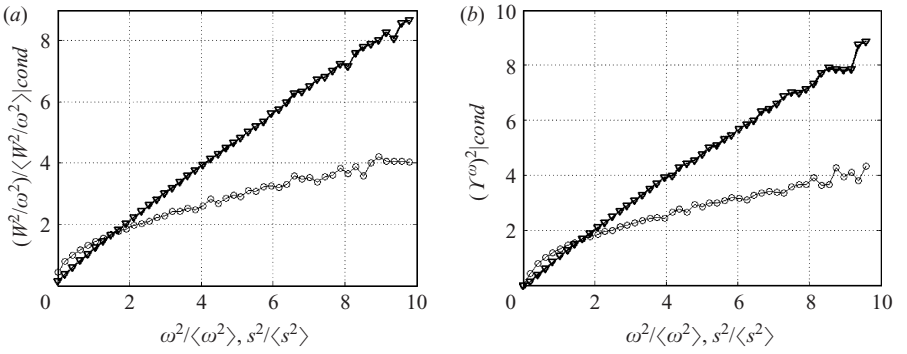

FIGURE 12. Conditional averages of (*a*) W^2/ω^2 and (*b*) $(\Upsilon^\omega)^2$ on $\circ$, ω^2; $\triangledown$, s^2.

3.3.2. *Reduction of nonlinearity*

Reduction of nonlinearity is understood here as in Tsinober (1998*a*, *b*, 2001) and Tsinober *et al.* (1999); that is, all the physically meaningful nonlinearities appear to be much smaller in the regions with concentrated vorticity (large enstrophy) than in the regions dominated by strain. This is true of such quantities as $\omega_i\omega_j s_{ij}$, $\omega_i\omega_j s_{ij}/\omega^2$, $s_{ij}s_{jk}s_{ki}$, $s_{ij}s_{jk}s_{ki}/s^2$, W^2, $(W_i \equiv \omega_j s_{ij})$, W^2/ω^2, $s_{ij}s_{jk}s_{im}s_{jm}$, $s_{ij}s_{jk}s_{im}s_{jm}/s^2$ and $(\Upsilon^\omega)^2 \equiv W^2/\omega^2 - \{\omega_i\omega_j s_{ij}/(\omega^2)\}^2$. All these quantities and others appear in the equations for vorticity, ω_i, enstrophy, ω^2, total strain, $s^2 = s_{ij}s_{ij}$, and higher-order quantities (e.g. Appendix 3 in Tsinober 2001). The quantity $(\Upsilon^\omega)^2$ is a measure of the inviscid rate of change of direction of the vorticity vector. The vector $\Upsilon_i^\omega = (1/\omega)\omega_k s_{ik} - (\omega_i/\omega^3)\omega_j\omega_k s_{jk}$ appears in the equation for the unit vector of vorticity, $\widetilde{\omega}_i = \omega_i/\omega$, i.e. it is responsible for tilting of vorticity. We show two examples in figure 12, clearly demonstrating the phenomenon of reduction of nonlinearity in the above sense.

Reduction of nonlinearity in the sense discussed above is seen even better looking at conditional means of separate eigen-contributions. Two examples, $\omega_i\omega_k s_{ik}/\omega^2$, and W^2/ω^2 are shown in figure 13.

3.3.3. *Geometrical statistics*

The issues described above are closely related to what is called geometrical statistics, which exhibits important aspects of dynamics and structure of turbulent flows. This includes important geometrical relations (such as alignments mentioned below) of dynamical significance owing to the essentially three-dimensional nature of turbulent flows.

The first example is the most dynamically important alignment between vorticity, $\boldsymbol{\omega}$, and the vortex stretching vector, $\boldsymbol{W}$, $W_i = \omega_j s_{ij}$, since the cosine of the angle between the two is the normalized enstrophy production, $\omega_i\omega_j s_{ij}/(\omega W)$. The PDF of the cosine of this angle, $\cos(\boldsymbol{\omega}, \boldsymbol{W})$, is positively skewed in full accordance with the predominance of the vortex stretching over vortex compressing (see figure 14*a*). This asymmetry is preserved at a very low level of enstrophy and total strain, which is a clear indication that there are no regions in the turbulent flow exhibiting Gaussian behaviour and/or which are 'structureless'.

The asymmetry in the PDF of $\cos(\boldsymbol{\omega}, \boldsymbol{W})$ is stronger in the regions dominated by strain, $s^2 \equiv s_{ij}s_{ij}$, than in the regions with large enstrophy, ω^2. This difference is smaller than in the DNS of Navier–Stokes equations at $Re_\lambda \sim 80$ (Tsinober *et al.* 1997, 1999; Tsinober 1998*a*). The most probable reason is that in the field experiment the velocity derivatives are somewhat under-resolved, especially in the regions with

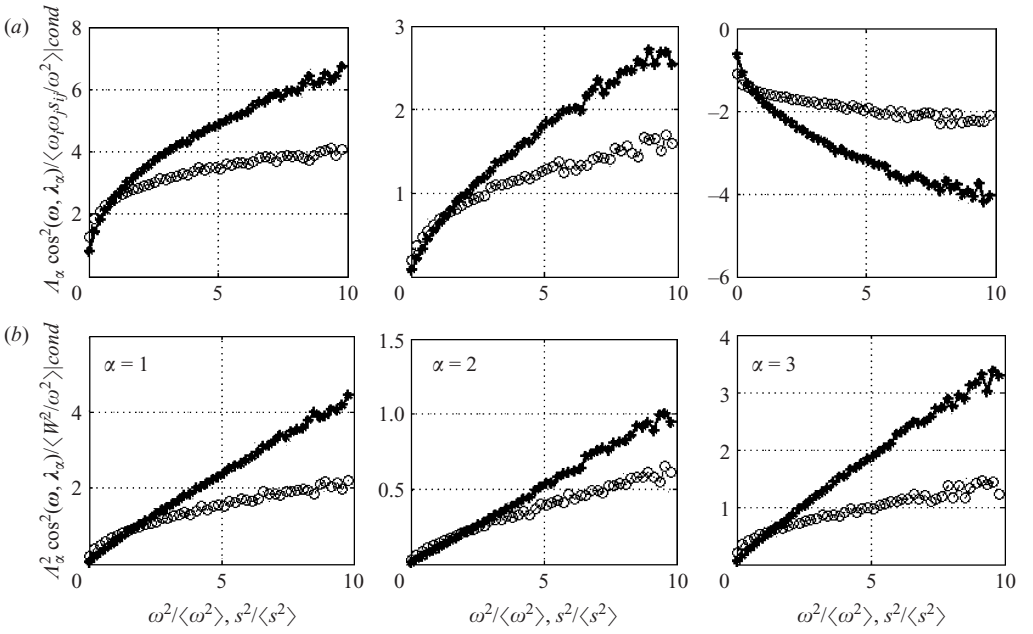

FIGURE 13. Conditional averages of eigen-contributions to (*a*) $\omega_i\omega_k s_{ik}/\omega^2$ and (*b*) W^2/ω^2. ○, conditional on ω; +, on s.

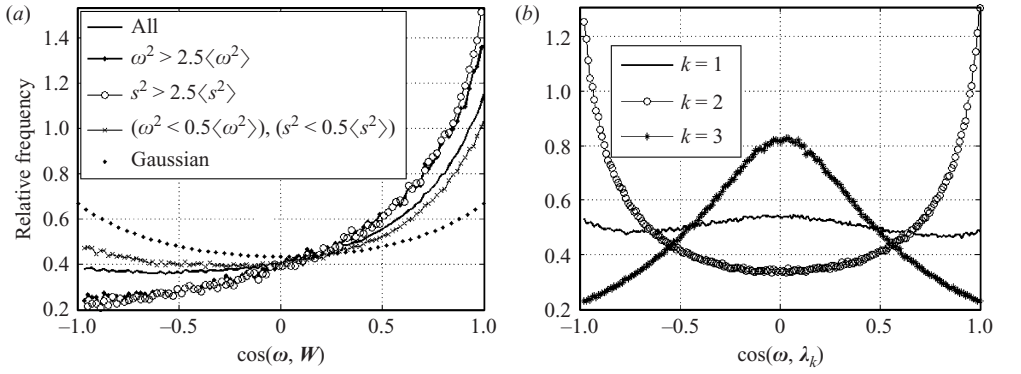

FIGURE 14. (*a*) PDF of the cosine between the vorticity vector, $\boldsymbol{\omega}$, and the vortex stretching vector, $\boldsymbol{W}$ and (*b*) between $\boldsymbol{\omega}$ and the eigenvectors, $\boldsymbol{\lambda}_k$, of the rate of strain tensor.

large enstrophy and/or strain, so the errors are likely to contribute to the 'blur' of the orientations. The stronger asymmetry in the PDF of $\cos(\boldsymbol{\omega}, \boldsymbol{W})$ in the regions, dominated by strain, than in the regions with large enstrophy corresponds to the above-mentioned reduction of nonlinearity in the regions with large enstrophy as compared to the regions dominated by strain.

Now let us consider the vorticity vector, $\boldsymbol{\omega}$, in the frame of the eigenvectors, $\boldsymbol{\lambda}_k$, of the rate of strain tensor, s_{ij}, with the corresponding eigenvalues, Λ_k, ordered as $\Lambda_1 > \Lambda_2 > \Lambda_3$. Figure 14(*b*) shows the PDFs of $\cos(\boldsymbol{\omega}, \boldsymbol{\lambda}_k)$. They exhibit the same behaviour as in the flows at moderate Reynolds numbers $Re_\lambda \sim 10^2$. The distributions

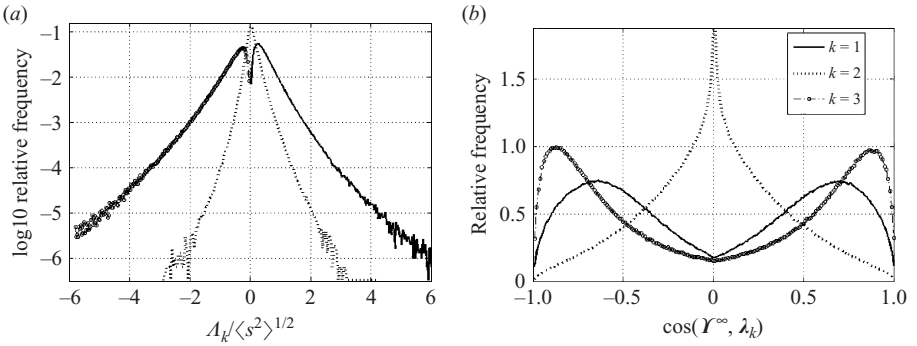

FIGURE 15. (*a*) PDF of the eigenvalues, Λ_k, of the rate of strain tensor, s_{ij} and (*b*) PDF of the cosine between the vector $\boldsymbol{\Upsilon}^\omega$ and the eigenvectors, $\boldsymbol{\lambda}_k$, of the rate of strain tensor.

are clearly symmetric, and there is strong preferential alignment between $\boldsymbol{\omega}$ and $\boldsymbol{\lambda}_2$, the eigenvector corresponding to the intermediate eigenvalue, Λ_2.

The enstrophy production can be expressed in the eigenframe as

$$\omega_i\omega_k s_{ik} = \omega^2\Lambda_1\cos^2(\boldsymbol{\omega}, \boldsymbol{\lambda}_1) + \omega^2\Lambda_2\cos^2(\boldsymbol{\omega}, \boldsymbol{\lambda}_2) + \omega^2\Lambda_3\cos^2(\boldsymbol{\omega}, \boldsymbol{\lambda}_3).$$

An important aspect is that the asymmetry of $\cos(\boldsymbol{\omega}, \boldsymbol{W})$ and the corresponding process of predominant production of enstrophy is associated with two qualitatively different regions of turbulent flow. The first one is where vorticity is aligned with $\boldsymbol{\lambda}_1$, the eigenvector corresponding to the largest eigenvalue, Λ_1, of s_{ij}. The second region is where vorticity tends to be aligned with $\boldsymbol{\lambda}_2$. We emphasize that the contribution to the enstrophy production and other nonlinearities from the first region is about three times larger than that from the second region, in spite of the general tendency for alignment between vorticity and $\boldsymbol{\lambda}_2$ (see figure 14*b*). We point to at least two reasons for this. First, the second eigenvalue, Λ_2, though positively skewed, takes both positive and negative values (figure 15*a*), whereas Λ_1 assumes only positive values. Secondly, the magnitude of Λ_1 is much larger than that of Λ_2 (see table 5).

As mentioned, another aspect of geometrical statistics concerns the change of direction of vorticity, which is naturally characterized by the rate of change of the unit vector along the vorticity, $\widehat{\boldsymbol{\omega}} = \boldsymbol{\omega}/\omega$. There are two contributions to this rate: the inviscid and the viscous. The latter is inaccessible in our experiments. The former is equal to the vector $\Upsilon_i^\omega = (1/\omega)\omega_k s_{ik} - (\omega_i/\omega^3)\omega_j\omega_k s_{jk}$. The alignments, i.e. the PDFs of $\cos(\boldsymbol{\Upsilon}^\omega, \boldsymbol{\lambda}_k)$ of this vector with the eigenframe of the rate of strain tensor are shown in figure 15(*b*).

3.4. *Non-locality*

Our concern here is with the aspects which can be defined as direct coupling of large and small scales (Praskovsky *et al.* 1993; Kholmyansky & Tsinober 2000).

In figure 16, we show some results similar to those obtained by Praskovsky *et al.* (1993) (figure16*a*) in parallel with those conditioned on the magnitude of the vector of velocity fluctuations, u, where $u^2 = u_1^2 + u_2^2 + u_3^2$. A similar behaviour is observed for conditional statistics of $\langle \delta u_i^n \rangle$ for all $i = 1, 2, 3$ and $n = 2, 3, 4$.

Two aspects deserve a special comment. First, there is a clear tendency of increase of the conditional averages of the structure functions with the energy of fluctuations, as is seen from figure 16(*b*). Secondly, such a tendency, indicative of direct coupling, is observed also for the smallest distance $\sim \eta$, which was used for estimates of the derivatives in the streamwise direction. This result is reliable owing to the absence

Value at the height (m)	α	0.8	1.2	2.0	3.0	4.5	7.0	10.0
	1	1.44	1.60	1.36	1.31	1.53	1.04	1.37
$\langle\omega^2\Lambda_\alpha\cos^2(\boldsymbol{\omega},\boldsymbol{\lambda}_\alpha)\rangle$	2	0.44	0.62	0.67	0.46	0.46	0.58	0.49
	3	−0.87	−1.22	−1.03	−0.77	−0.99	−0.62	−0.85
	1	0.53	0.33	0.29	0.52	0.46	0.49	0.49
$\langle\omega^2\Lambda_\alpha^2\cos^2(\boldsymbol{\omega},\boldsymbol{\lambda}_\alpha)\rangle$	2	0.09	0.05	0.15	0.14	0.13	0.16	0.15
	3	0.38	0.63	0.56	0.34	0.41	0.35	0.36
	1	1.77	1.56	1.63	1.91	2.08	1.55	2.19
$\langle\Lambda_\alpha\cos^2(\boldsymbol{\omega},\boldsymbol{\lambda}_\alpha)\rangle$	2	0.47	0.50	0.52	0.45	0.47	0.54	0.47
	3	−1.24	−1.07	−1.15	−1.36	−1.55	−1.09	−1.66
	1	0.51	0.50	0.50	0.51	0.49	0.50	0.49
$\langle\Lambda_\alpha^2\cos^2(\boldsymbol{\omega},\boldsymbol{\lambda}_\alpha)\rangle$	2	0.08	0.09	0.10	0.10	0.10	0.11	0.10
	3	0.41	0.41	0.41	0.40	0.41	0.40	0.41
	1	0.53	0.52	0.51	0.49	0.47	0.51	0.47
$\langle\Lambda_\alpha\rangle/\langle s^2\rangle^{1/2}$	2	0.09	0.10	0.09	0.07	0.06	0.09	0.06
	3	−0.62	−0.61	−0.60	−0.56	−0.53	−0.60	−0.53
	1	0.40	0.39	0.40	0.40	0.41	0.40	0.41
$\langle\Lambda_\alpha^2\rangle/\langle s^2\rangle$	2	0.04	0.04	0.04	0.05	0.05	0.04	0.06
	3	0.56	0.57	0.56	0.55	0.55	0.56	0.55
	1	0.48	0.53	0.54	0.52	0.76	0.46	0.60
$\langle\Lambda_\alpha^3\rangle/\langle s^2\rangle^{3/2}$	2	0.01	0.02	0.02	0.02	0.01	0.02	0.02
	3	−0.73	−0.82	−0.83	−0.86	−1.19	−0.80	−1.04

TABLE 5. Contribution of terms, associated with the eigenvalues, Λ_α, of s_{ij}, to the mean enstrophy generation, $\langle\omega_i\omega_j s_{ij}\rangle = \langle\omega^2\Lambda_i\cos^2(\boldsymbol{\omega},\ \boldsymbol{\lambda}_i)\rangle$, and vortex stretching, $\langle W^2\rangle = \langle\omega^2\Lambda_i^2\cos^2(\boldsymbol{\omega},\ \boldsymbol{\lambda}_i)\rangle$, at various heights from the field experiment. There is no summation over the number of the eigenvector, α. The last three triads of rows show the means, the mean squares and the mean cubes of the eigenvalues of the rate of strain tensor, Λ_α; $s^2 = s_{ij}s_{ij} = \Lambda_1^2 + \Lambda_2^2 + \Lambda_3^2$; $s_{ij}s_{jk}s_{ki} = \Lambda_1^3 + \Lambda_2^3 + \Lambda_3^3$.

of problems in estimating the derivatives in the streamwise direction (contrary to the other two directions).

In figure 17, we show also similar conditional statistics for the enstrophy, ω^2, and the total strain, $s_{ij}s_{ij}$. The result is similar to that shown in figure 16 for the smallest distance $\sim\eta$ and to that of Kholmyansky & Tsinober (2000).

4. Concluding remarks

The results obtained in this work are in full conformity with those obtained in a similar field experiment. Being the first repetition of an experiment of this kind (in which explicit information is obtained on the field of velocity derivatives) it gives us confidence in both experiments. The results reported here confirm the main conclusions made before. Namely, these results are similar to those obtained in experiments in laboratory turbulent grid flow and in DNS of Navier–Stokes equations in a cubic domain with periodic boundary conditions, both at $Re_\lambda \sim 10^2$. An important aspect is that this similarity is not only qualitative, but, to a large extent, quantitative. The main difference between the two is in the 'length' of the inertial range. This means that the basic physics of turbulent flow at high Reynolds number $Re_\lambda \sim 10^4$, at least qualitatively, is the same as at moderate Reynolds numbers, $Re_\lambda \sim 10^2$. This is true of such basic processes as enstrophy and strain production, geometrical statistics, the

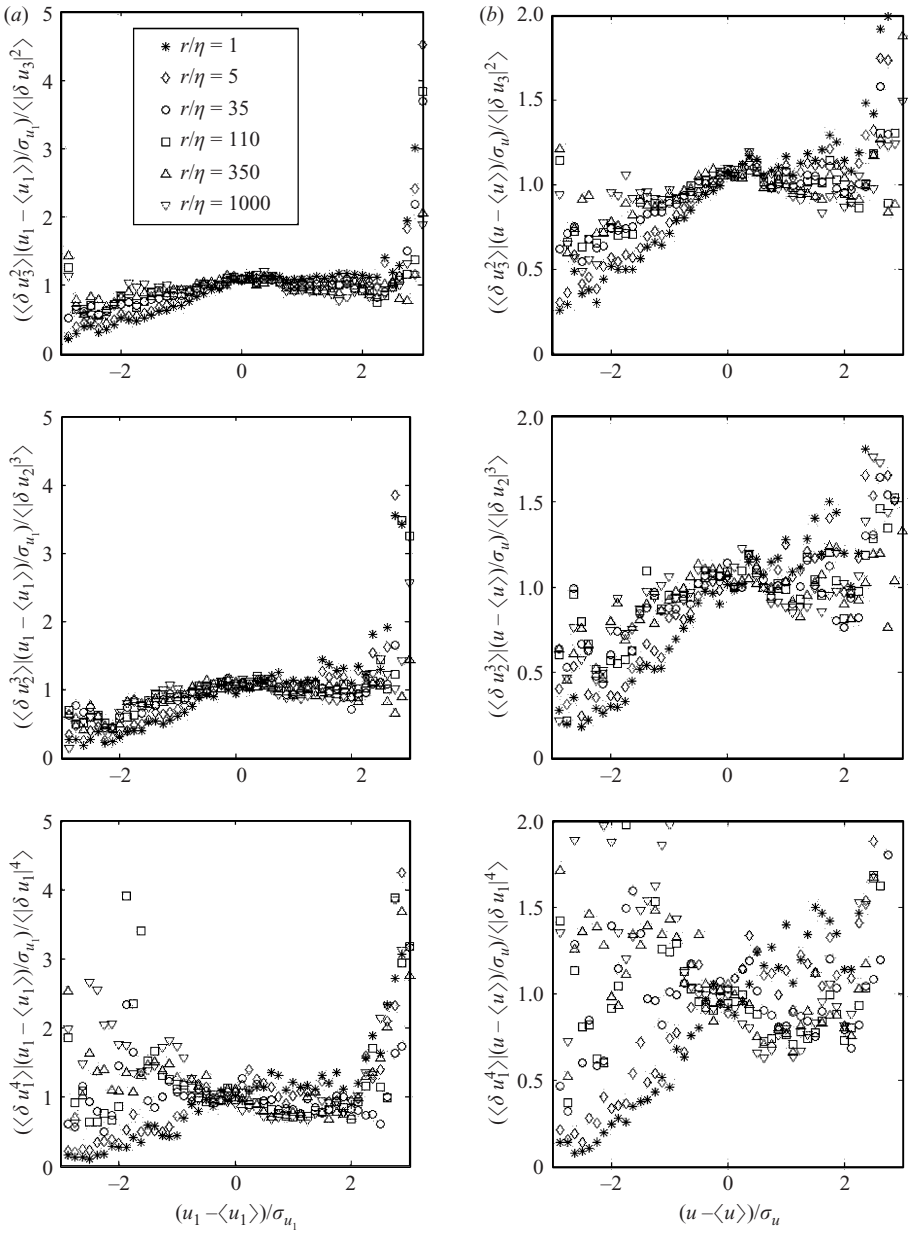

FIGURE 16. Conditional averages of velocity increments, $\langle \delta u_i^n \rangle = \langle (u_i(x + r) - u_i(x))^n \rangle$, (*a*) conditioned on the fluctuation of u_1 and (*b*) on the magnitude of the vector of velocity fluctuations, u.

role of concentrated vorticity and strain, reduction of nonlinearity and some non-local effects.

The next point is that the present experiments went far beyond the previous ones in two main respects. The first one is that all the data were obtained without invoking the Taylor hypothesis and therefore a variety of results on fluid particle accelerations became possible. The second is simultaneous measurements of temperature and its

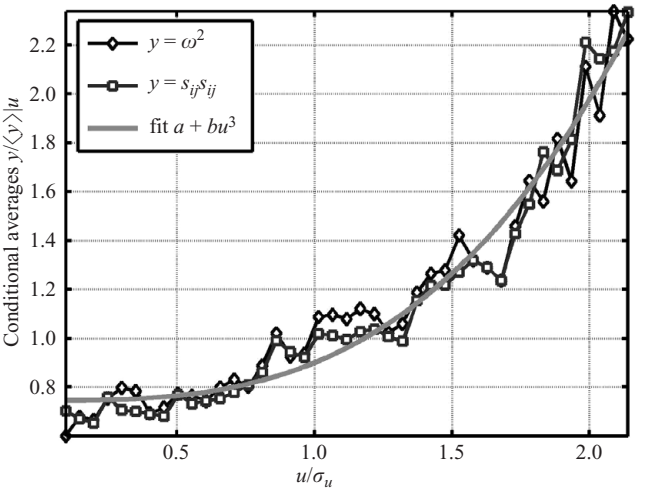

FIGURE 17. Conditional averages of enstrophy, ω^2, and total strain, $s_{ij}s_{ij}$, on magnitude of velocity fluctuations vector, u. The fit is in the spirit of the Kolmogorov refined similarity hypothesis, though it is a fit in the first place. This fit cannot be expected to be universal quantitatively and should at least have different coefficients a and b for flows with different large-scale properties in the spirit of the Landau remark. $a = 0.746$; $b = 0.154$.

gradients with the emphasis on joint statistics of temperature and velocity derivatives. Both are reported in Parts 2 and 3.

This work was supported in part by the Israel Science Foundation (ISF), founded by the Israel Academy of Sciences and Humanities, Research grant 34/02 and the United States – Israel Binational Science Foundation (BSF), No. 2002264. The field experiment in Switzerland was supported by the Vice President for Research of ETH, Zürich.

The authors appreciate the assistance provided by Dr K. W. Hoyer and Mr T. Blunschi from ETH.

REFERENCES

ANTONIA, R. A. & CHAMBERS, A. J. 1980 On the correlation between turbulent velocity and temperature derivatives in the atmospheric surface layer. *Boundary-Layer Met.* **18**, 399–410.

BUSEN, R., GULITSKY, G., KHOLMYANSKY, M., SCHUMANN, U., TSINOBER, A. & YORISH, S. 2001 An airborne experiment on turbulent velocity derivatives. Final Report for the German Israeli Foundation, Grant no. I-541-132.08/97.

CHERTKOV, M., PUMIR, A. & SHRAIMAN, B. I. 1999 Lagrangian tetrad dynamics and the phenomenology of turbulence. *Phys. Fluids* **11**, 2394–2410.

CRAWFORD, A. M., MORDANT, N. & BODENSCHATZ, E. 2005 Joint statistics of the Lagrangian acceleration and velocity in fully developed turbulence. *Phys. Rev. Lett.* **94**, 024501/1–4.

GALANTI, B. & TSINOBER, A. 2000 Self-amplification of the field of velocity derivatives in quasi-isotropic turbulence. *Phys. Fluids* **12**, 3097–3099; erratum *Phys. Fluids* **13**, 1063 (2001).

GALANTI, B., GULITSKY, G., KHOLMYANSKY, M., TSINOBER, A. & YORISH, S. 2003 Velocity derivatives in turbulent flow in an atmospheric boundary layer without Taylor hypothesis. In *Turbulence and Shear Flow Phenomena* (ed. N. Kasagi, J. K. Eaton, R. Friedrich, J. A. C. Humphrey, M. A. Leschziner & T. Miyauchi), vol. 2, pp. 745–750.

GALANTI, B., GULITSKY, G., KHOLMYANSKY, M., TSINOBER, A. & YORISH, S. 2004 Joint statistical properties of fine structure of velocity and passive scalar in high Reynolds number flows. *Adv. Turb.* **10**, 267–270.

Gibson, C. H., Stegen, G. R. & Williams, R. B. 1970 Statistics of the fine structure of turbulent velocity and temperature fields measured at high Reynolds number. *J. Fluid Mech.* **41**, 153–168.

Gulitski, G., Kholmyansky, M., Kinzelbach, W., Lüthi, B., Tsinober, A. & Yorish, S. 2007*a* Velocity and temperature derivatives in high-Reynolds-number turbulent flows in the atmospheric surface layer. Part 2. Accelerations and related matters. *J. Fluid Mech.* **589**, 83–102.

Gulitski, G., Kholmyansky, M., Kinzelbach, W., Lüthi, B., Tsinober, A. & Yorish, S. 2007*b* Velocity and temperature derivatives in high-Reynolds-number turbulent flows in the atmospheric surface layer. Part 3. Temperature and joint statistics of temperature and velocity derivatives. *J. Fluid Mech.* **589**, 103–123.

Jimenes, J., Wray, A. A., Saffman, P. G. & Rogallo, R. S. 1993 The structure of intense vorticity in homogeneous isotropic turbulence. *J. Fluid Mech.* **255**, 65–90.

Kerr, R. M. 1985 Higher-order derivative correlations and the alignment of small-scale structures in isotropic numerical turbulence. *J. Fluid Mech.* **153**, 31–58.

Kholmyansky, M. & Tsinober, A. 2000 On the origins of intermittency in real turbulent flows. In *Proceedings of the Symposium on Intermittency in turbulent flows and other dynamical systems held at Isaac Newton Institute, Cambridge, June 21–24, 1999* (ed. J. C. Vassilicos). Isaac Newton Institute for Mathematical Sciences, Preprint NI99017-TRB. Cambridge University Press.

Kholmyansky, M., Tsinober, A. & Yorish, S. 2000 Geometrical statistics in the atmospheric turbulent flow at $Re_\lambda = 10^4$. *Adv. Turb.* **8**, 895–898.

Kholmyansky, M., Tsinober, A. & Yorish, S. 2001*a* Velocity derivatives in the atmospheric surface layer at $Re_\lambda = 10^4$. *Phys. Fluids* **13**, 311–314.

Kholmyansky, M., Tsinober, A. & Yorish, S. 2001*b* Velocity derivatives in the atmospheric surface layer at $Re_\lambda = 10^4$. Further results. In *Proceedings of the Second International Symposium on Turbulence and Shear Flow Phenomena, Stockholm, June, 27–29, 2001* (ed. E. Lindborg, A. Johansson, J. Eaton, J. Humphrey, N. Kasagi, M. Leschziner & M. Sommerfeld), vol. 1, pp. 109–113.

Kolmogorov, A. N. 1941*a* The local structure of turbulence in incompressible viscous fluid for very large Reynolds numbers. *Dokl. Akad. Nauk SSSR* **30**, 299–303; for English translation see: *Selected works of A. N. Kolmogorov*, vol. 1 (ed. V. M. Tikhomirov), pp. 312–318, 1991. Kluwer.

Kolmogorov, A. N. 1941*b* Dissipation of energy in locally isotropic turbulence. *Dokl. Akad. Nauk SSSR* **32**, 19–21; for English translation see: *Selected works of A. N. Kolmogorov*, vol. 1 (ed. V. M. Tikhomirov), pp. 324–327, 1991. Kluwer.

Lüthi, B., Tsinober, A. & Kinzelbach, W. 2005 Lagrangian measurement of vorticity dynamics in turbulent flow. *J. Fluid Mech.* **528**, 87–118.

Mordant, N., Delour, J., Léveque, E., Michel, O., Arnéodo, A. & Pinton, J.-F. 2003 Lagrangian velocity fluctuations in fully developed turbulence: scaling, intermittency, and dynamics. *J. Stat. Phys.* **113**, 701–717.

Mordant, N., Crawford, A. M. & Bodenschatz, E. 2004*a* Experimental Lagrangian acceleration probability density function measurement. *Physica* D **193**, 245–251.

Mordant, N., Crawford, A. M. & Bodenschatz, E. 2004*b* Three-dimensional structure of the Lagrangian acceleration in turbulent flows. *Phys. Rev. Lett.* **93**, 214501/1–4.

Mordant, N., Lévêque, E. & Pinton, J.-F. 2004*c* Experimental and numerical study of the Lagrangian dynamics of high Reynolds turbulence. *New J. Phys.* **6**, 116/1–44.

Praskovsky, A., Gledzer, E. B., Karyakin, M. Yu. & Zhou, Y. 1993 Fine-scale turbulence structure of intermittent shear flows. *J. Fluid Mech.* **248**, 493–511.

Report 2003 *Velocity and temperature derivatives in high Reynolds number turbulent shear flow. Joint field experiment, Sils-Maria 2003-4*. Faculty of Engineering, Tel Aviv University and Institute for Hydromechanics and Water Management, Swiss Federal Institute of Technology, report.

Sandham, N. & Tsinober, A. 2000 Kinetic energy, enstrophy and strain rate in near-wall turbulence. *Adv. Turb.* **8**, 407–410.

Sreenivasan, K. R. & Antonia, R. 1997 The phenomenology of small-scale turbulence. *Annu. Rev. Fluid Mech.* **29**, 435–472.

Taylor, G. I. 1937 The statistical theory of isotropic turbulence. *J.Aeronaut. Sci.* **4**, 311–315.

Taylor, G. I. 1938 Production and dissipation of vorticity in a turbulent fluid. *Proc. R. Soc. Lond.* A **164**, 15–23.

Tennekes, H. & Lumley, J. L. 1972 *A First Course in Turbulence*. MIT Press.

Tsimanis, Y. 2005 Reproducibility of multi-hot-wire measurements in turbulent flows. Master's thesis Department of Fluid Mechanics and Heat Transfer, Faculty of Engineering, Tel Aviv University.

Tsinober, A. 1998*a* Is concentrated vorticity that important? *Eur. J. Mech. Fluids* **17**, 421–449.

Tsinober, A. 1998*b* Turbulence – beyond phenomenology. In *Chaos, Kinetics and Nonlinear Dynamics in Fluids and Plasmas* (ed. S. Benkadda & G. M. Zaslavsky), pp. 85–143. Springer.

Tsinober, A. 2001 *An Informal Introduction to Turbulence*. Kluwer.

Tsinober, A., Kit, E. & Dracos, T. 1992 Experimental investigation of the field of velocity gradients in turbulent flows. *J. Fluid Mech.* **242**, 169–192.

Tsinober, A., Shtilman, L. & Vaisburd, H. 1997 A study of vortex stretching and enstrophy generation in numerical and laboratory turbulence. *Fluid Dyn. Res.* **21**, 477–494.

Tsinober, A., Ortenberg, M. & Shtilman, L. 1999 On depression of nonlinearity in turbulence. *Phys. Fluids* **11**, 2291–2297.

Tsinober, A., Vedula, P. & Yeung, P. K. 2001 Random Taylor hypothesis and the behavior of local and convective accelerations in isotropic turbulence. *Phys. Fluids* **13**, 1974–1984.

Van Atta, C. W. & Antonia, R. A. 1980 Reynolds number dependence of skewness and flatness factors of turbulent velocity derivatives. *Phys. Fluids* **23**, 252–257.

Vedula, P. & Yeung, P. K. 1999 Similarity scaling of acceleration and pressure statistics in numerical simulations of isotropic turbulence. *Phys. Fluids* **11**, 1208–1220.

Vedula, P., Yeung, P. K. & Fox, R. O. 2001 Dynamics of scalar dissipation in isotropic turbulence: a numerical and modelling study. *J. Fluid Mech.* **433**, 29–60.

Yaglom, A. M. 1949 On the local structure of a temperature field in a turbulent flow. *Dokl. Akad. Nauk SSSR* **69**, 743–746. German translation: Jaglom, A. M. 1958 Über die locale Struktur des Temperaturfeldes einer turbulenten Strömung, *Sammelband zur Statistischen Theorie der Turbulenz*, Akademie-Verlag, Berlin, pp. 141–146.